

Document downloaded from:

<http://hdl.handle.net/10251/168336>

This paper must be cited as:

Salvador, F.J.; Gimeno, J.; Martín, J.; Carreres, M. (2020). Thermal effects on the diesel injector performance through adiabatic 1D modelling. Part I: Model description and assessment of the adiabatic flow hypothesis. *Fuel*. 260:1-13.  
<https://doi.org/10.1016/j.fuel.2019.116348>



The final publication is available at

<https://doi.org/10.1016/j.fuel.2019.116348>

Copyright Elsevier

Additional Information

1 **THERMAL EFFECTS ON THE DIESEL INJECTOR PERFORMANCE THROUGH ADIABATIC 1D**  
2 **MODELLING. PART I: MODEL DESCRIPTION AND ASSESSMENT OF THE ADIABATIC FLOW**  
3 **HYPOTHESIS**

4 **Salvador, F.J., Gimeno, J., Martín, J., Carreres, M. (\*)**.

5 CMT-Motores Térmicos, Universitat Politècnica de València

6 Camino de Vera s/n, E-46022 Spain

7

8 (\*) Corresponding author:

9 Dr. Marcos Carreres, marcarta@mot.upv.es

10 CMT-Motores Térmicos, Universitat Politècnica de València

11 Camino de Vera s/n, E-46022 Spain

12 Telephone: +34-963876540

13 Fax: +34-963877659

14

15 **ABSTRACT**

16 The fuel flow along common-rail injectors is usually treated as isothermal, although the expansions across the injector  
17 orifices lead to variations in the fuel temperature that in turn modify the fuel properties influencing injector dynamics.  
18 This investigation introduces the hypothesis of adiabatic flow to account for local temperature variations in the  
19 computational model of a solenoid injector previously introduced by the authors in its isothermal variant. The main  
20 contribution of the study consists on the assessment of the validity of this hypothesis by qualitatively estimating the  
21 relative importance of the heat transfer processes during the injection event and in the time lapse among injections. Results  
22 of this tentative assessment for engine-like conditions imply that heat transfer is usually still occurring by the time of a  
23 new injection, meaning any initial temperature difference among the fuel and the injector wall is not expected to be  
24 completely mitigated before each injection event. The magnitude of reduction of this temperature difference depends on  
25 the injection frequency through engine speed and load. Anyway, the assumption of adiabatic flow seems to hold once the  
26 steady conditions of the injection are reached, meaning that any temperature change predictions considered with the  
27 adiabatic hypothesis may be valid as long as a certain temperature change is accounted for at the injector inlet. In a second  
28 part of the paper, the capabilities of this new model are validated against experimental data, allowing the use of the model  
29 to explore the influence of the thermal effects on the injection event.

30 **KEYWORDS**

31 diesel, injection, computational, 1D modelling, fuel temperature, adiabatic flow

32 **LIST OF NOTATION**

33  $A_o$  outlet area

34  $Ad$  adiabatic number

35  $B_s$  isentropic bulk modulus

36  $C_a$  area coefficient

37  $C_d$  discharge coefficient

38  $C_i$  coefficients for the fuel properties correlations

39  $C_v$  velocity coefficient

40  $c_p$  fluid heat capacity at constant pressure

41  $D$  orifice diameter

42  $e$  specific internal energy

43  $F_i$  coefficients for the fuel dynamic viscosity expression

44  $FO$  Fourier number

45  $f$  fuel properties correlation function

46  $h$  specific enthalpy

47  $h_t$  stagnation specific enthalpy

48  $J_0$  Bessel function of first kind of order zero

49  $K_{Ad}$  constant for the transient radial heat conduction in an injector duct

50  $k_f$  fuel thermal conductivity

51  $L$  orifice length

52  $m_i$  total mass injected per cycle

53  $\dot{m}_f$  fuel mass flow

54  $\dot{m}_{th}$  theoretical mass flow

55  $Nu$  Nusselt number

56  $n_e$  engine speed

57  $p$  pressure

58  $p_0$  reference pressure

59	$p_b$	injector backpressure
60	$p_{dw}$	downstream pressure
61	$p_i$	injection pressure
62	$p_{up}$	upstream pressure
63	$Pr$	Prandtl number
64	$r$	radial coordinate
65	$r_0$	cylinder diameter
66	$Re$	Reynolds number
67	$St$	Stanton number
68	$T$	temperature
69	$T_0$	reference temperature
70	$T_{dw}$	downstream temperature
71	$T_i$	fuel temperature at the injector inlet
72	$T_{up}$	upstream temperature
73	$T_w$	wall temperature
74	$t$	time
75	$t_k$	characteristic time of heat transfer due to conduction
76	$t_{res}$	fuel residence time in the injector
77	$u$	flow velocity
78	$u_{th}$	theoretical flow velocity
79	$v_f$	fuel specific volume
80	<b>GREEK SYMBOLS</b>	
81	$\alpha$	fuel thermal diffusivity
82	$\beta$	volumetric thermal expansion coefficient
83	$\varepsilon_{\Delta T}$	percentual deviation among the theoretical temperature change across an orifice and the experimental one
84	$\theta$	temperature difference among the fluid and the wall
85	$\theta_i$	initial temperature difference among the fluid and the wall
86	$\lambda_n$	eigenvalues for the problem of transient radial heating by conduction through an infinite cylinder
87	$\mu_f$	fuel absolute viscosity

88  $\mu_{f,0}$  fuel absolute viscosity at atmospheric pressure  
89  $\rho_f$  fuel density  
90  $\tau_{Ad}$  ratio among residence time and conduction characteristic time  
91 **ABBREVIATIONS**  
92 BMEP Brake Mean Effective Pressure  
93 DI Direct Injection  
94 ET Energizing Time  
95 OA control volume outlet orifice  
96 OZ control volume inlet orifice  
97 ROI Rate of Injection  
98

## 99 **1. INTRODUCTION**

100 The mixing process is key to the performance of direct-injection engines, due to its direct influence on the combustion  
101 phenomenon and therefore on the engine performance and the formation of emissions [1]. Some researchers have then  
102 focused on the fuel injection system, analysing the role of the injector topology [2,3], the nozzle geometrical features [4–  
103 8] and the operating conditions [9–11] on the injector internal flow, spray formation and fuel-air mixing processes. In the  
104 common-rail diesel engines community the gathered knowledge led, for instance, to a generalized progressive increase  
105 in the fuel injection pressure.  
106 Most studies in the literature focus on the nozzle internal flow and spray development, whereas the injector upstream flow  
107 has not been paid so much attention. Given that the injection event is a transient process and considering the high flow  
108 velocities through the injector and the small dimensions of its ducts, experimental observations in this regard present  
109 several difficulties. Nevertheless, the internal flow through the injector rules its own dynamics, especially in non-direct  
110 acting injectors [12]. This justifies the need for computational models as an approach to carry out research in the topic.  
111 In this regard, 1D modelling has been widely employed, allowing the study of the whole injection process at a low  
112 computational cost. Most investigations take the assumption that the flow along the injector is isothermal [13–15],  
113 including past investigations carried out by the authors [16–18]. However, the ultra-high pressures reached by current  
114 diesel injection systems [19] (up to 300 MPa) imply that the thermal effects taking place within the injector become  
115 relevant. Thus, there may be important fuel temperature variations along the injector due to friction heating or due to the  
116 important fuel depressurization that takes place at the injector flow restrictions (i.e. control volume orifices or most

117 importantly the nozzle [20–22]). The local changes in fuel temperature and pressure influence the fuel thermophysical  
118 properties that are a function of these thermodynamic variables, such as the speed of sound, density or viscosity [23].  
119 These properties, in turn, may impact the injected mass flow rate and spray development [24,25].  
120 Due to the aforementioned reasons, several modellers started accounting for local temperature variations in their models,  
121 considering the injector internal flow to be adiabatic [26,27], even though they covered a short range of injector operating  
122 conditions. CFD modellers also explored the thermal effects in diesel injectors. Theodorakakos et al. [20] focused on the  
123 nozzle flow, reporting that the flow could be either heated or subcooled at the nozzle outlet depending on the nozzle  
124 discharge coefficient and the flow regime induced by the injector operating conditions. On the other hand, Yu et al. [28]  
125 extended the modelling of thermal effects to diesel sprays injected through convergent-divergent nozzles even in  
126 cavitating conditions.  
127 Despite these efforts, few attempts have been made to contrast the calculated local temperature variations along the  
128 injector against results obtained experimentally in order to assess the hypothesis of adiabatic flow. Even though this  
129 hypothesis is undoubtedly more accurate than the isothermal assumption, it may not hold if the fuel is slowly injected  
130 into the combustion chamber letting heat transfer to take place with the surrounding atmosphere across the injector walls.  
131 The authors tried to qualitatively assess the validity of the adiabatic flow assumption through experimental measurements  
132 on diesel injector calibrated orifices [29]. These orifices were submitted to controlled pressure drops and the measured  
133 temperature variations were compared to the theoretical ones given by isenthalpic expansions. It was found that the flow  
134 through a diesel injector orifice could be regarded to as adiabatic for the operating conditions that led to low fuel residence  
135 times within it (most conditions found during the steady-state stage of the injection were found to fall in this category).  
136 Later, the authors implemented the adiabatic flow hypothesis in a CFD code and modelled these same calibrated orifices  
137 [22], reporting good agreement among the temperature variations predicted by the model and the experimental results.  
138 Then, the model was applied to the flow through diesel injection nozzles. Nevertheless, these investigations aimed at the  
139 study of a single injection event, without taking into account the time lapse among injections. Depending on the injection  
140 frequency induced by the operating conditions, heat transfer may take place during this period modifying the inlet fuel  
141 temperature prior to each injection.  
142 This study deals with the implementation of the adiabatic flow assumption in a diesel injector 1D model, so that the model  
143 accounts for local temperature variations along the injector. The present paper describes the theoretical foundation for  
144 this implementation on an existing 1D model of a Bosch CRI 2.20 diesel injector previously presented by the authors in  
145 its isothermal variant [18]. Most importantly, a discussion on the validity of the adiabatic hypothesis for the injector

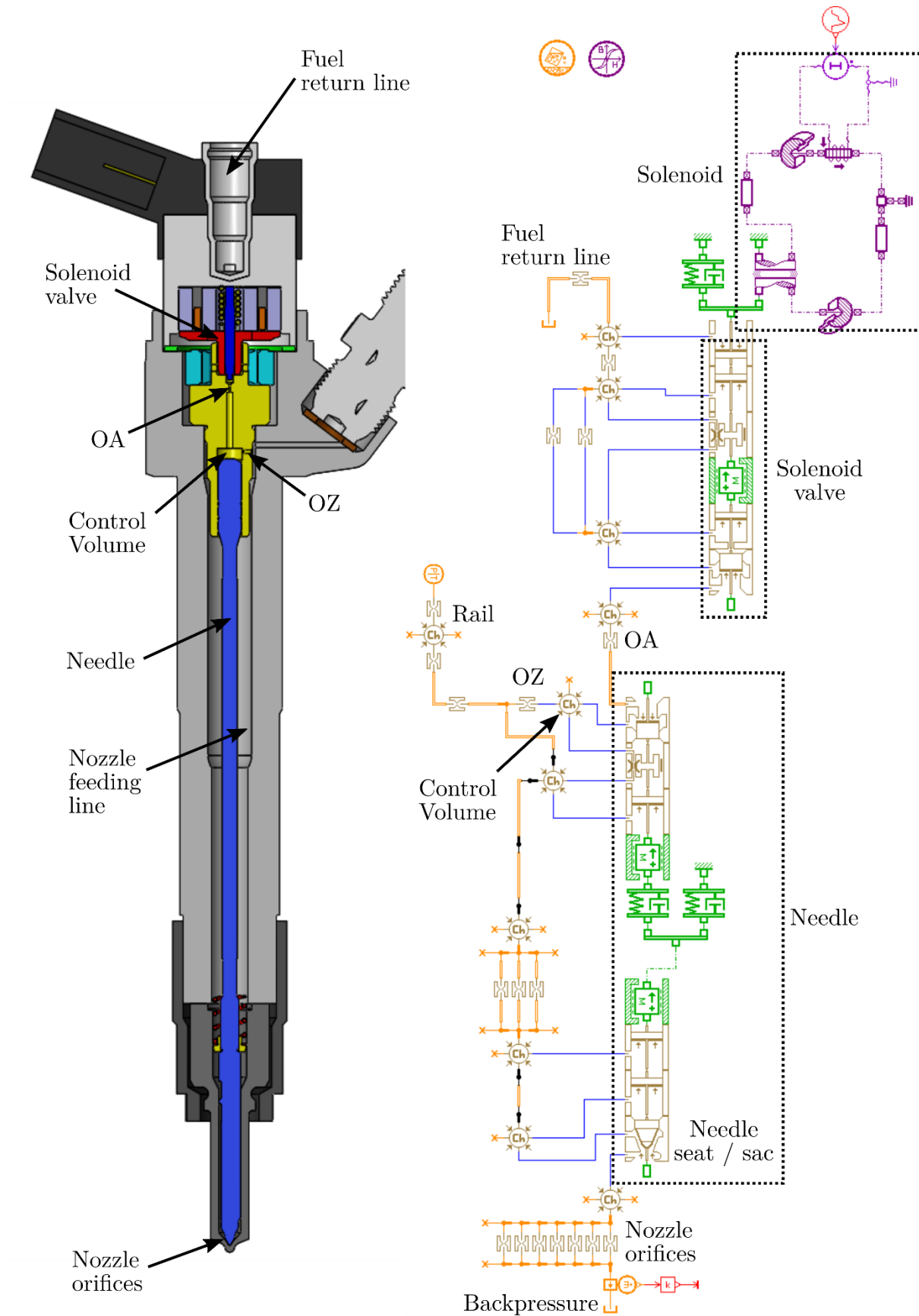
146 internal flow is presented. This consists on estimating, from a qualitative point of view, which operating conditions (both  
147 for a real engine and for the injection rate and visualization measurements typically performed for the study of the  
148 injection process in laboratory environments) could lead to accepting or refusing the adiabatic flow hypothesis with more  
149 confidence.

150 A second part of the paper [30] shows a thorough practical validation of the adiabatic model covering the predictions of  
151 mass flow rate and temperature change through the orifices, the total injected mass per cycle and the pressure wave  
152 transmission along the injector. It then analyses the results purely provided by the validated model. This includes the fuel  
153 temperature variations along the injector ducts and orifices and the extent of their influence on the injection phenomenon,  
154 including the analysis of the impact of the fuel temperature on the effectiveness to split injections when using multiple  
155 injection strategies.

156

## 157 **2. DESCRIPTION OF THE INJECTOR 1D MODEL**

158 The computational investigation has been carried out based on a Bosch CRI 2.20 injector. This common-rail injector is  
159 driven by a solenoid valve and is ballistic (which means that the mechanical needle lift limit is not reached during the  
160 usual operation of the injector). As it has been said, the assumption of adiabatic flow has been implemented in a 1D model  
161 of this injector that was already introduced by the authors in previous investigations [18]. In the previous version of the  
162 model, the fuel flow was assumed to be isothermal. Therefore, the fuel temperature was considered to be constant along  
163 the injector ducts during the complete injection event. This meant that all the significant fuel properties (i.e. speed of  
164 sound, density and viscosity) remained unaltered both spatially and temporally. In the present investigation, local  
165 variations of the fuel temperature and its associated properties are considered during the injection by means of the  
166 adiabatic flow assumption introduced in the model. This model was implemented in AMESim, a commercial platform  
167 for multi-domain simulation [31].



168

169 Figure 1. Bosch CRI 2.20 injector diagram and AMESim model sketch.

Salvador, F.J., Gimeno, J., Martín, J., Carreres, M., "Thermal effects on the diesel injector performance through adiabatic 1D modelling. Part I: Model description and assessment of the adiabatic flow hypothesis", Fuel 260:116348 (author version).

doi: 10.1016/j.fuel.2019.116348



170 A complete sketch of the internal parts of the injector is shown in **Figure 1**, together with their equivalence in the adiabatic  
171 AMESim model. When the injector is energized, the fuel flowing along the injector is submitted to several hydraulic  
172 restrictions on its path from the injector inlet to any possible outlet:

- 173 • Part of the flow from the injector inlet flows directly towards the nozzle orifices through the *nozzle feeding line*.
- 174 • Part of the flow from the injector inlet enters the control volume through the OZ orifice (also known as *control*  
175 *volume inlet orifice*). This fuel flow can in turn follow 2 different paths: on the one hand, part of the fuel leaks  
176 through the gap among the needle and the control volume piece, lubricating the needle and feeding the nozzle  
177 orifices; on the other hand, part of the fuel flows through the OA orifice (also known as *control volume outlet*  
178 *orifice*) and leaves the injector through the *fuel return line*.

179 The internal dimensions and relevant hydraulic parameters were introduced to the model after a thorough geometrical and  
180 hydraulic characterization. The geometrical characterization included a complete metrology of the internal parts of the  
181 injector carried out according to the techniques described in [32]. On the other hand, the hydraulic characterization  
182 consisted on experimentally determining the evolution of the discharge coefficient with  $Re$  for the most relevant flow  
183 restrictions. This included the characterization of the cavitation phenomenon, found for the control volume outlet orifice  
184 (OA). For more details on this characterization and the model parameters, please refer to the already mentioned previous  
185 work by the authors [18]. The main features of the model are summarized as follows:

- 186 • The elastic deformations of the mechanical movable pieces are modelled, as a key factor to properly predict the  
187 injection delay (once the injector is energized, the elastic deformation of the needle must be recovered prior to  
188 the new injection event).
- 189 • Pressure wave transmission is modelled through the injector internal lines. To do so, the deformation of the  
190 pieces shaping the injector ducts is considered by means of the material modulus of compressibility. These  
191 factors, together with an accurate description of the fuel speed of sound evolution with the pressure and  
192 temperature, are mandatory to properly predict the time among injections when using split injection strategies.
- 193 • Friction among mechanical elements is accounted for, together with the friction among the fuel and the  
194 mechanical elements. Fuel leakage among elements is also considered.
- 195 • The discharge coefficient of the orifices is computed at each time step as a function of the local  $Re$  established  
196 [33]. The effect of cavitation in the discharge coefficient behaviour is also considered. Possible reductions in  
197 area in the orifices due to the lift of mechanical valves are taken into account as well.
- 198 • As it has been stated, the relevant fuel properties depend on the local temperature (thanks to the assumption of

199           adiabatic flow) and pressure and are also varied temporally.

200   It is important to remark that the model accounts for the hydraulic, mechanical and electromagnetic phenomena relevant  
201   in the actuation of this solenoid diesel injector, but the local temperature changes are only included in the hydraulic  
202   components in what constitutes the assumption of adiabatic fuel flow here assessed. In Part II, these local changes in fuel  
203   temperature are shown to present an important influence on the hydraulics dominating the dynamics of the injector needle  
204   [30]. The assumption of adiabatic flow, on the other hand, implies that the temperature of the mechanical and  
205   electromagnetic metallic components is assumed to remain constant. This could have relevant implications in the case of  
206   the needle. As far as the solenoid valve is concerned, it only lifts to a maximum of around 20  $\mu\text{m}$  [18], which is achieved  
207   almost instantaneously once the solenoid is energized (and almost instantaneously closed back towards its seat once de-  
208   energized). The evolution of this valve in different families of solenoid injectors shows that its influence on the injection  
209   rate curve from one generation to another is limited [34], making it safe to assume that any variations of the  
210   electromagnetic properties of a given valve related to its possible metal temperature changes are small compared to the  
211   influence of the hydraulics in the control volume piloting the needle.

### 212   **3. IMPLEMENTATION OF THE ADIABATIC FLOW ASSUMPTION**

213   As stated previously, the implemented model accounts for local variations in fuel temperature and pressure during the  
214   injection event. All the fuel temperature changes along the injector are computed assuming adiabatic flow, with no  
215   interaction with the surroundings in terms of heat transfer.

216   In absence of external work, the first law of thermodynamics establishes that the total enthalpy or stagnation enthalpy ( $h_t$ )  
217   of a fluid is conserved during an adiabatic process, as shown in Eq. (1):

$$\Delta h_t = \Delta \left( h + \frac{u^2}{2} \right) = 0 \quad (1)$$

218   where  $h$  is the fluid specific enthalpy and  $u$  its velocity.

219   Along any hydraulic component (such as an orifice submitted to a pressure drop or a hydraulic line with an associated  
220   loss due to friction) within the injector, Eq. (1) may be rewritten as:

$$h(T_{dw}, p_{dw}) = h(T_{up}, p_{up}) - \frac{1}{2} \Delta u^2 \quad (2)$$

221   Used by the model, Eq. (2) implies that the temperature downstream (i.e. at the outlet) of any hydraulic component may  
222   be computed if the upstream temperature (i.e. at the inlet), the pressure drop and the velocity change across the component  
223   are known, as long as the fuel specific enthalpy has been expressed as a function of the pressure and temperature (the

224 particular dependency used in this investigation is introduced in Section 3.1). This includes the flow through the small  
225 calibrated orifices (OZ, OA and nozzle orifices) and the flow through long ducts along which pressure losses are expected  
226 (for instance, the nozzle feeding line).

227 It is interesting to analyse Eq. (2) in the view of the important restrictions to the flow along the injector, since this will  
228 allow understanding in Section 3.1 which locations and under which circumstances the fuel may heat up or cool down:

229 • In the case of the particular components where the velocity change is not relevant (as it happens along the nozzle  
230 feeding line), Eq. (2) leads to the conservation of specific enthalpy in order to calculate the temperature change  
231 through them:

$$h(T_{dw}, p_{dw}) \approx h(T_{up}, p_{up}) \quad (3)$$

232 • In the case of other hydraulic components, the established pressure drops are very high (such as the nozzle  
233 orifices and the OA orifice). Thus, the velocity upstream of them is small compared to the downstream velocity.  
234 Therefore, Eq. (2) can be approximated as follows:

$$h(T_{dw}, p_{dw}) \approx h(T_{up}, p_{up}) - \frac{1}{2} u_{dw}^2 \quad (4)$$

235 It is then possible to introduce a velocity coefficient [35] similar to the one defined by Siebers [36]:

$$C_v = \frac{u}{u_{th}} \quad (5)$$

236 where  $u_{th}$  is the theoretical velocity according to Bernoulli:

$$u_{th} = \sqrt{\frac{2(p_{up} - p_{dw})}{\rho_f}} \quad (6)$$

237 According to these definitions, Eq. (4) can be rewritten to yield the downstream temperature in terms of the  
238 pressure drop and the velocity coefficient:

$$h(T_{dw}, p_{dw}) \approx h(T_{up}, p_{up}) - C_v^2 \frac{(p_{up} - p_{dw})}{\rho_f} \quad (7)$$

239 Furthermore, the velocity coefficient can be expressed in terms of the discharge coefficient and the area  
240 coefficient [35]:

$$C_d = C_v \cdot C_a \quad (8)$$

241 where the area coefficient is defined in an analogous manner to the velocity coefficient so that it takes into  
242 account the area contraction in an orifice (relevant when cavitation appears), whereas the discharge coefficient  
243 is defined as the ratio among the actual mass flow rate through an orifice and the theoretical one, as shown by

244 Eq. (9):

$$C_d = \frac{\dot{m}_f}{A_0 \sqrt{2 \rho_f (p_{up} - p_{dw})}} \quad (9)$$

245 Therefore, Eq. (7) can also be expressed in terms of the discharge coefficient and the area coefficient:

$$h(T_{dw}, p_{dw}) \approx h(T_{up}, p_{up}) - \left(\frac{C_d}{C_a}\right)^2 \frac{(p_{up} - p_{dw})}{\rho_f} \quad (10)$$

246 In this investigation, the fuel density has been taken at a mean pressure and mean temperature among the ones  
247 found at the inlet and the outlet of the corresponding orifice. It is important to note that Eq. (1), upon which the  
248 adiabatic assumption has been implemented, applies with no work exchange among the hydraulic restriction and  
249 other components of the system. This statement is acceptable for most cases, but it may not be true in the case  
250 of the nozzle orifices for the transient stages. For the low values of needle lift of these stages, the needle might  
251 exchange mechanical work with the nozzle. Nevertheless, the interaction among needle and nozzle flow is only  
252 deemed to be relevant for values of needle lift lower than 75  $\mu\text{m}$  [37], which are usually restricted to a time in  
253 the order of 0.1 ms for both the opening and the closing stages [18]. Thus, this phenomenon is restricted during  
254 the injection event and the assumption is not expected to importantly influence the results. In any case, the results  
255 reported in Part II [30] are restricted to the steady-state stage of the injection.

### 256 3.1. Fuel model

257 The equations derived in Section 3 highlight the need to express the fuel specific enthalpy as a function of temperature  
258 and pressure in order to compute the temperature variations across an injector hydraulic component with the adiabatic  
259 flow assumption. The fuel specific enthalpy may be related to its specific internal energy according to Eq. (11):

$$h = e + \frac{p}{\rho_f} \quad (11)$$

260 Let us now evaluate the derivative of the fuel specific enthalpy as a function of temperature and pressure:

$$dh = \left(\frac{\partial h}{\partial T}\right)_p dT + \left(\frac{\partial h}{\partial p}\right)_T dp = c_p dT + \frac{1}{\rho_f} \left[1 + \frac{T}{\rho_f} \left(\frac{\partial \rho_f}{\partial T}\right)_p\right] dp \quad (12)$$

261 Introducing the volumetric thermal expansion coefficient:

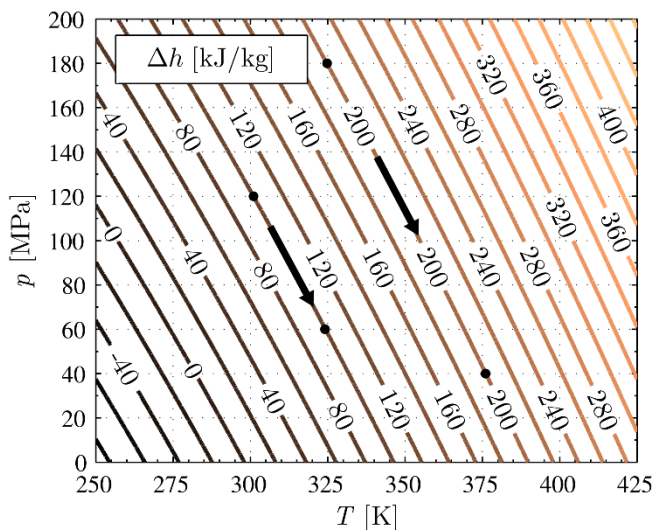
$$\beta = \frac{1}{v_f} \left(\frac{\partial v_f}{\partial T}\right)_p = -\frac{1}{\rho_f} \left(\frac{\partial \rho_f}{\partial T}\right)_p \quad (13)$$

262 Eq. (12) can then be written in terms of  $\beta$ :

$$dh = c_p dT + \frac{(1 - \beta T)}{\rho_f} dp \quad (14)$$

263 Please note that the second term of the right hand side of Eq. (14) would be zero for an ideal gas (for which  $\beta \cdot T = 1$ ), but  
264 cannot be neglected for a liquid. Eq. (14) can be integrated if the fuel properties evolution with the pressure and  
265 temperature is known.

266 A winter diesel fuel has been considered for the computational study, replicating the fuel utilized in the experiments used  
267 for the model validation later explained in Section 5 [38]. Some of its properties (namely speed of sound, bulk modulus  
268 and density) were experimentally characterized by the authors for the range of pressures and temperatures of interest for  
269 common-rail systems [23]. As far as the heat capacity at constant pressure ( $c_p$ ) is concerned, its evolution with the pressure  
270 was assimilated to the ISO 4113 test fluid one [39], whereas its dependency with the temperature was estimated from  
271 pure alkanes [40,41]. This assumption is not deemed to introduce a noticeable error, given the low variation of  $c_p$  for  
272 diesel fuels on the relevant range of temperatures [42,43]. It is possible to use these data in Eq. (14): specific enthalpy  
273 variations ( $\Delta h$ ) can be determined among conditions by taking small variations of temperature ( $\Delta T$ ) and pressure ( $\Delta p$ )  
274 instead of differentials. This allows to build the *specific enthalpy map* of the fuel, as shown in **Figure 2**.



275  
276 Figure 2. Lines of iso-specific enthalpy as a function of temperature and pressure for the winter diesel fuel. Reference  
277 conditions for  $h = 0$  J/kg:  $T_0 = 298$  K;  $p_0 = 0.1$  MPa.

278 As it has been commented, in the case of the hydraulic components of the injector through which the flow velocity change  
279 is not relevant, Eq. (3) practically leads to the conservation of specific enthalpy ( $\Delta h \approx 0$ ). Thus, across such a component  
280 (for instance, along the nozzle feeding line) the flow could be regarded to as isenthalpic and the temperature change due

281 to a pressure loss would be directly given by **Figure 2**. In these cases, **Figure 2** illustrates that the fuel would warm upon  
282 expansion, as opposed to what happens to an ideal gas, due to the existence of the second term of right hand side of Eq.  
283 (14). Hence, for example, an isenthalpic expansion from 120 MPa to 60 MPa with an upstream temperature of 300 K  
284 would lead to a downstream temperature of 325 K ( $\Delta T = 25$  K), or an isenthalpic expansion from 180 MPa to 40 MPa  
285 with an upstream temperature of 325 K would lead to a downstream temperature of 375 K ( $\Delta T = 50$  K). This makes sense  
286 in the view of Eq. (11): under the assumption of adiabatic flow, the heating induced by viscous dissipation or a fuel  
287 depressurization is assumed to remain within the fluid, contributing to increase its internal energy. As a consequence, in  
288 the case of an isenthalpic expansion, the fluid temperature rises as it expands. In addition, the higher the fuel temperature  
289 is, the more accused the slope of the iso-enthalpy lines in **Figure 2**. This means that, for isenthalpic expansions with a  
290 given pressure drop, higher temperature rises will be achieved with a low upstream temperature.

291 In the general case for which the stagnation enthalpy is preserved, the temperature change also depends on the flow  
292 velocity change along the process. As given by Eq. (2), an increase in fluid velocity due to a depressurization (for instance  
293 across the nozzle orifices) would lead to a reduction in specific enthalpy downstream of the orifice. According to **Figure**  
294 **2**, this reduction in specific enthalpy would imply a reduction in fluid temperature. Therefore, the net change in fluid  
295 temperature given by Eq. (2) could be positive or negative depending on the magnitude of the velocity change across the  
296 restriction. In the case of the nozzle orifices and the OA orifice, as developed in Eq. (10), this dependency of the fuel  
297 temperature on the velocity increase can also be expressed in terms of the pressure drop and the discharge coefficient.  
298 This reasoning is consistent with 3D CFD calculations by the authors in a previous work [22] concerning the flow along  
299 the orifices of a nozzle with a high discharge coefficient. In this work, a temperature increase was observed at the orifice  
300 walls (shear, low-velocity zones) with a temperature decrease at the centre of the orifice. Overall, the fuel bulk temperature  
301 decreased along the orifice, as the 1D computation would suggest through Eq. (9) for an orifice with a high discharge  
302 coefficient submitted to an important pressure drop.

303 The evolution of each of the fuel properties with the temperature and pressure was provided to AMESim, so that their  
304 local variations are considered. Specifically, the fuel density, speed of sound and bulk modulus dependency with  
305 temperature and pressure were introduced in the form of the polynomial expressions given by Eq. (15), whose coefficients  
306 were fitted on the basis of experimental data, as shown in a previous work by the authors [23]:

$$f(T, p) = C_0 + C_1(T - T_0) + C_2(p - p_0) + C_3(T - T_0)(p - p_0) + C_4(T - T_0)^2 + C_5(p - p_0)^2 \quad (15)$$

307 where  $f$  denotes either the fuel density, speed of sound or isentropic bulk modulus.

308 As far as the fuel viscosity is concerned, experimental measurements were only available at atmospheric pressure [22].

309 Thus, dynamic viscosity was introduced as a function of the temperature according to the correlation shown in Eq. (16):

$$\mu_{f,0}(T) = F_1 e^{F_2(T-T_0)} \quad (16)$$

310 The evolution of the dynamic viscosity with the pressure was estimated according to the Kouzel expression [44],  
 311 reproduced in Eq. (17):

$$\mu_f(p, T) = \frac{\mu_{f,0}}{1000} \cdot 10^{\left[\left(\frac{p-0.10133}{1000}\right)^{-1.48+5.86\mu_{f,0}^{0.181}}\right]} \quad (17)$$

312 The coefficients  $C_i$  or  $F_i$  used for these correlations are summarized for each property in **Table 1**, together with the  $R^2$   
 313 values reported.

Property	$C_0$ [-]	$C_1$ [-]	$C_2$ [-]	$C_3$ [-]	$C_4$ [-]	$C_5$ [-]	$F_1$ [-]	$F_2$ [-]	$R^2$ [-]
$a_f$ [m/s]	1350.59	-3.1485	4.4928	0.0074	0	-0.0070	-	-	0.9996
$\rho_f$ [kg/m <sup>3</sup> ]	826.54	-1.021	0.603	0.0014	0.00125	-0.00083	-	-	0.9995
$B_s$ [MPa]	$1.489 \cdot 10^9$	$-8.766 \cdot 10^6$	$1.199 \cdot 10^7$	0	0	-7461.3	-	-	0.9998
$\mu_{f,0}$ [Pa·s]	-	-	-	-	-	-	3.2158	-0.0263	0.9906

314 Table 1. Coefficients for the fuel properties correlations of Eq. (15). Each fuel property is given in the referred units  
 315 introducing  $T$  in K and  $p$  in MPa. Reference conditions:  $T_0 = 298$  K;  $p_0 = 0.1$  MPa.

316

#### 317 4. DISCUSSION: ON THE VALIDITY OF THE ASSUMPTION OF ADIABATIC FLOW

318 Before applying the adiabatic assumption to the flow along the injector, it is key to assess the limits of the extension of  
 319 this hypothesis. In the frame of the present work, this assessment can ensure the reliability of the simulations performed  
 320 by the computational model, given that local changes in temperature and pressure are taken into account. More generally,  
 321 this assessment can be a contribution of interest to both experimentalists and modellers in the field that usually require  
 322 the injector outlet temperature as an input or boundary condition to their studies. It is thus interesting to evaluate the  
 323 validity of this hypothesis considering the injector flow in both the typical engine-like operating conditions and the usual  
 324 operating conditions reproduced in laboratory environments to conduct measurements such as the rate of injection curve  
 325 or spray visualization by means of experimental test rigs. These kinds of measurements have become usual to evaluate  
 326 the injector performance [45–48] and the spray development and mixing characteristics [49]. The rate of injection  
 327 measurements have indeed been used to validate the computational model of this investigation in the second part of the  
 328 paper [30]. In any case, it must be pointed out that the assessment here presented has been carried out in qualitative terms,  
 329 comparing the relative importance among phenomena and providing with orders of magnitude for their relevance.

330 The qualitative evaluation of the validity of this assumption has been divided into the analysis during the injection event  
 331 itself (when the fuel is flowing, while the injector is energized) and the analysis of relevance of heat transfer to or from

332 the fuel during the time among successive injections (where the fuel is at rest).

#### 333 4.1. During the injection

334 The validity of the hypothesis while the fuel is effectively flowing through the most important injector internal orifices  
335 was already qualitatively assessed experimentally by the authors [29], considering that the most important thermal effects  
336 will take place in these restrictions given the pressure drops induced by them. The most relevant features of that work are  
337 next summarized for continuity in the discussion presented in the present paper. Specifically, continuous flow was  
338 established along the control volume orifices of the Bosch CRI 2.20 injector and a Denso G4S injector. In the facility, a  
339 given single orifice could be isolated, with its inlet connected to an accumulating rail by a high-pressure hydraulic line  
340 and its outlet connected to a discharge volume through another high-pressure line with identical diameter. The flow could  
341 then be submitted to different controlled pressure drops across the orifices. Then, the temperature was measured at two  
342 different locations (one in the hydraulic line 16 cm upstream of the orifice and the other in the hydraulic line 16 cm  
343 downstream of the orifice) where the controlled flow was assumed to be developed and attained a similar velocity. Under  
344 these conditions, according to Eq. (2), the flow is forced to be virtually isenthalpic (Eq. (3)). This implies that the  
345 theoretical fuel temperature change across the orifice is given by an isenthalpic evolution as the ones depicted in **Figure**  
346 **2** (always leading to heating among these 2 locations). Therefore, the temperature changes measured for different  
347 operating conditions could be compared to the theoretical ones predicted by Eq. (2). The deviations could then be  
348 attributed to heat exchange with the surroundings. The analysis of these deviations gave a hint on the conditions that led  
349 to heat exchange becoming more or less relevant to the problem.

350 In this regard, the dimensionless parameter defined in Eq. (18) was theoretically derived to account for all the variables  
351 that influenced the proneness of the flow through an orifice to exchange heat with the surroundings:

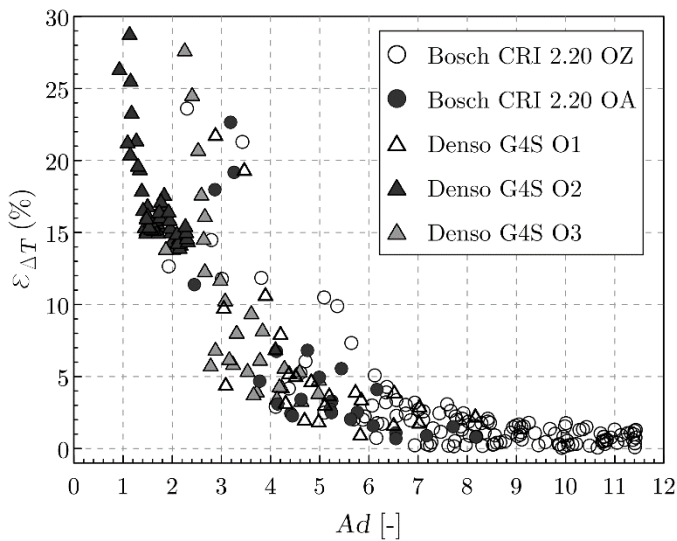
$$Ad = \frac{1}{4} \frac{D}{L} St^{-1} = \frac{1}{4} \frac{D}{L} \frac{Pr Re}{Nu} \quad (18)$$

352 Please note that  $Ad$  is a corrected  $St$  number with a fourth of the  $D/L$  ratio of dimensions. For details on this derivation  
353 and the significance of the  $D/L$  factor, the reader may refer to the complete previous study [29].

354 The different diameter of the internal orifices and the different conditions (i.e. pressure drops) tested were associated to  
355 several values of  $Ad$ . **Figure 3** shows how the percentual deviation ( $\epsilon_{\Delta T}$ ) among the theoretical temperature change and  
356 the experimental one were found to evolve with the  $Ad$  parameter for the non-cavitating conditions tested (the flow  
357 through the orifices of a Denso G4S injector was also studied in order to gather further data). It was observed that most  
358 points corresponding to the same  $Ad$  value collapse to similar values of  $\epsilon_{\Delta T}$  regardless the combination of orifice and



359 condition tested. Thus,  $Ad$  can be considered as a good indicator of the proneness of the flow through an orifice to  
360 exchange heat with the surroundings.



361

362 Figure 3. Percentual deviation  $\varepsilon_{\Delta T}$  among the theoretical temperature change and the experimentally determined one for  
363 the  $Ad$  values induced by each non-cavitating condition tested for each orifice (data for the Bosch CRI 2.20 and the Denso  
364 G4S injector orifices). Data from [29].

365 The main finding of the investigation was that low values of  $Ad$  lead to a high departure to the temperature change  
366 predicted by the theoretical adiabatic expansion, whereas these deviations are bounded for high  $Ad$  values: the deviations  
367 are generally lower than 10% for  $Ad > 4$  and lower than 5% for  $Ad > 6$ . It may then be stated that:

- 368
- For a given orifice, the tendency of the flow across it to exchange heat with the surroundings depends on the  
369 established value of  $Re/Nu$  and the flow regime. Empirical correlations in the literature relate  $Nu$  to  $Re$  (among  
370 other factors). These correlations depend on the flow regime, but generally establish  $Nu = a \cdot Re^b$ , where  $b < 1$   
371 [50,51]. Hence,  $Ad$  is higher the greater  $Re$ . The significance of this fact may be analysed as follows. Low values  
372 of  $Re$  yielding low values of  $Ad$  are associated to low flow velocities, implying high residence times for the fuel  
373 in the ducts. Hence, heat transfer is allowed to take place. Consequently, low pressure drops through an orifice  
374 induce a higher interaction with the ambient than high pressure drops. On the contrary, high flow velocities are  
375 induced for high pressure drops leading to high values of  $Re$  and  $Ad$ . In these conditions, it is possible to neglect  
376 the heat transfer and to assume that all the heat generated due to the fluid expansion remains within the fluid,  
377 being invested in raising its temperature.
  - For a given operating condition (associated to a particular pressure drop across the orifices), the orifice diameter  
378 also influences the proneness of the flow across it to exchange heat, not only due to its impact through  $Re$  and  
379  $Nu$ . The term  $D/L$  is relevant in  $Ad$  since, for a particular channel length, a lower diameter implies greater wall  
380

381 effects. On the one hand, this is explained by a higher proportion of the flow being in touch with the orifice  
382 surface, interacting with the surroundings. On the other hand, the boundary layer is also proportionally thicker,  
383 meaning that its viscous effects will reduce the flow velocity close to the orifice walls, increasing the fuel  
384 residence times and favouring heat transfer.

385 In consequence, the flow established through the injector orifices with operating conditions leading to high average values  
386 of  $Ad$  behaves in a nearly adiabatic manner. In this regard, it was found that the diameter of the Bosch CRI 2.20 control  
387 volume orifices was large enough to obstruct the heat transfer process during a given expansion, unless the pressure drop  
388 was too low. It was checked that pressure drops in the order of the ones imposed during the steady stage of the injection  
389 lead to large enough values of  $Ad$ <sup>1</sup>. During the transient stages of opening and closing this assumption could not be true,  
390 although the characteristic times of these stages are way lower than the time lapse among injections dealt with in the next  
391 subsection.

## 392 4.2. During the time lapse among injections

### 393 4.2.1. Theoretical approach

394 Both in real engine-like operating conditions and controlled experimental environments, an important temperature  
395 difference may be established among the fuel (stored in a tank far from the injector) and the injector walls (located close  
396 to the engine head, significantly warmer during the engine operation). Injection in real engine conditions, with fuel being  
397 injected into the cylinder in a pulsed manner and remaining at rest during the lapse among injections, is a transient  
398 phenomenon. This transiency, together with the amount of varied operating conditions that may be achieved during an  
399 engine run, hinders the analysis. The approach taken in this study to qualitatively assess whether the heat transfer is  
400 relevant is to compare the fuel residence time in the injector ( $t_{res}$ ) to a characteristic time of heat transfer due to conduction  
401 from the injector walls to the fuel ( $t_k$ ). Hence, a dimensionless parameter  $\tau_{Ad}$  has been defined as the ratio among times,  
402 as given by Eq. (19):

$$\tau_{Ad} = \frac{t_{res}}{t_k} \quad (19)$$

403 The parameter  $\tau_{Ad}$  allows evaluating the importance of heating among injections to establish the relative importance of  
404 the thermal effects during the injection, so that:

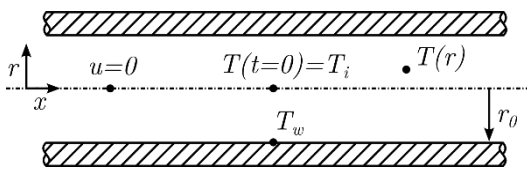
---

<sup>1</sup>As an example, Part II [30] shows that for a fairly low rail pressure of 40 MPa (a limiting case in terms of absolute pressure drop along the orifices, since the injector does not open properly for rail pressures below 30 MPa) the pressure drop along the Bosch CRI 2.20 OZ orifice is around 12 MPa. The associated  $Ad$  established along the OZ orifice is about 6.2.

- 405
- If  $\tau_{Ad} \ll 1$ , the fuel residence time in the injector is way lower than the characteristic time of heat transfer and  
406 the fuel does not significantly modify its temperature during the time lapse among injections. Once an injection  
407 starts, the fuel will modify its temperature due to its internal evolution along the injector (i.e. expansions across  
408 the orifices) or will exchange heat with the ambient depending on the related  $Ad$  value, as analysed earlier.  
409 Anyway, low values of  $Ad$  are not expected if  $t_{res} \ll t_k$ , since low fuel residence times imply either high injection  
410 frequencies (limited to 4000 rpm in diesel engines) or large pressure gradients that would lead to high  $Ad$   
411 numbers by definition. Therefore, the assumption of adiabatic flow does not seem to be compromised at any  
412 stage for low values of  $\tau_{Ad}$ .
  - If  $\tau_{Ad} \approx 1$ , the fuel residence times are similar to the characteristic time of heat transfer and the fuel importantly  
413 changes its temperature during the lapse among injections. Hence, the temperature of the fuel inside the injector  
414 has enough time to get closer to the injection wall temperature prior to each injection event. At the same time,  
415 this means that the temperature difference between the wall and the fluid is minimized by the time an injection  
416 starts. For this reason, the ability of the fuel to modify its temperature upon its internal expansions (retaining the  
417 heat within itself in what would constitute an adiabatic process) or to transfer this heat to the ambient can be  
418 assumed to depend on the related values of the  $Ad$  number.
  - If  $\tau_{Ad} \gg 1$ , the fuel residence times are much higher than the characteristic times of heat transfer. Thus, by the  
420 time of a new injection, the heat transfer process will be completed and the fuel temperature will already coincide  
421 with the injector wall temperature at all locations. During the injection itself, the assumption of adiabatic flow  
422 still depends on the  $Ad$  number: please note that the situation of  $t_{res} \gg t_k$  could be generated either by very low  
423 injection frequencies (not usual in diesel engines) or by small pressure gradients piloting the injector. On the one  
424 hand, high  $Ad$  values could still be reached during the injection (for instance, for high values of rail pressure)  
425 regardless how low the injection frequency was. This fact, together with the non-existent temperature difference  
426 among the fuel and the wall by the time of a new injection would still support the assumption of adiabatic flow  
427 during the injection. On the other hand, as seen in Section 4.1, the case of low values of  $Ad$  could lead to the fuel  
428 not being able to retain the temperature changes produced by its internal evolution through the hydraulic  
429 restrictions even though the temperature difference between the wall and the fluid upstream of the restriction  
430 was negligible. In this latter case, the assumption of adiabatic flow during the injection would no longer be valid.
- 432 The characteristic time of heat transfer due to conduction from the injector walls ( $t_k$ ) has been estimated considering the  
433 simplified problem of transient radial conduction in an infinitely long cylinder as the one shown in **Figure 4**, which will

434 then be assimilated to the injector nozzle feeding line (since it is the most relevant line in terms of fuel volume and where  
 435 the effects of heat transfer both among injections and during the injection itself, if any, would be more noticeable). Even  
 436 though the problem is not generic and the geometry of the infinitely long cylinder importantly departs from the reality  
 437 present in the nozzle feeding line (recall Figure 1) of the Bosch CRI 2.20 diesel injector, this provides an analytical  
 438 solution to be used as a reference. Additionally, the nozzle feeding line of most commercial solenoid-operated injectors  
 439 is a cylindrical duct (2<sup>nd</sup> generation Bosch solenoid injectors [52] prior to the present Bosch CRI 2.20, Denso [53], Delphi  
 440 [54], etc.). Thus, this analysis is assumed to give a representative order of magnitude of the heat transfer from the injector  
 441 walls in the time lapse among injections that could be used for qualitative comparison with the fuel residence times in the  
 442 injector. In any case, the impact of assuming a cylindrical duct instead of an annular one on the calculated values of  $t_k$  and  
 443  $\tau_{Ad}$  is analysed in Section 4.2.2 through the results of a transient heat transfer simulation.

444 Assuming the cylindrical shape, the fluid temperature at the centre of the cylinder initially takes a value  $T_i$ , whereas the  
 445 wall remains at its own temperature  $T_w$ . The fluid is considered to be at rest so that convection is negligible. The  
 446 assumption of infinite length ensures one-dimensional conduction in the radial direction. Once the fluid temperature is  
 447 let to evolve freely, it will modify its value  $T(r)$  along the cylinder radial coordinate  $r$ , tending to approach the wall  
 448 temperature. These hypotheses conform the scenario in which heat transfer takes place in an easier way (any heat flux  
 449 among the fluid and the walls is only pointed in the radial direction), thus leading to the minimum possible characteristic  
 450 times for heat transfer,  $t_k$ . This results in a conservative estimation of  $\tau_{Ad}$ .



451  
 452 Figure 4. Scheme of an infinitely long cylinder containing fuel at rest.

453 Before an injection event, the fuel (which entered the injector at a certain temperature) remains at rest and is able to  
 454 exchange heat with the injector walls (at a different temperature). For any radial position, the temperature difference may  
 455 be defined in Eq. (20):

$$\theta(r) = |T(r) - T_w| \quad (20)$$

456 Eq. (21) describes the problem in cylindrical coordinates:

$$\frac{1}{\alpha} \frac{\partial \theta}{\partial t} = \frac{\partial^2 \theta}{\partial r^2} + \frac{1}{r} \frac{\partial \theta}{\partial r} \quad (21)$$

457 where  $\alpha$  is the fuel thermal diffusivity. With the boundary conditions  $\theta(r = r_0) = 0$ ;  $\left(\frac{\partial\theta}{\partial r}\right)_{r=0} = 0$ ; and  $\theta(t = 0) = \theta_i$ ,  
 458 the general solution for  $\theta(r,t)$  is given by Eq. (22):

$$\theta(r, t) = \sum_{n=1}^{\infty} \theta_i J_0(\lambda_n r) e^{-\lambda_n^2 \alpha t} \quad (22)$$

459 where  $J_0$  is the Bessel function of first kind of order zero and  $\lambda_n$  are the problem eigenvalues, which are the roots of  
 460  $J_0(\lambda_n r_0) = 0$ . For instance, the first roots are  $\lambda_1 r_0 = 2.4048$ ;  $\lambda_2 r_0 = 5.5201$ ; and  $\lambda_3 r_0 = 8.6537$ . Eq. (22) shows that  
 461 the fluid temperature at the cylinder axis  $T(0,t)$  will exponentially tend to the wall temperature. It is then possible to  
 462 determine a relaxation time (which can be assimilated to  $t_k$ ) for which  $T(0,t)$  has almost reached this asymptotic condition.  
 463 The first root ( $\lambda_1 r_0 = 2.4048$ ) leads to the longer relaxation time and must then be the one used in its determination.  
 464 Focusing at the cylinder axis ( $r = 0$ ) where  $J_0 = 1$ , the first particular solution from Eq. (22) yields:

$$\frac{\theta(0, t)}{\theta_i} = e^{-\lambda_1^2 \alpha t_k} \quad (23)$$

465 From where the time may be isolated:

$$t_k = -\ln \left[ \frac{\theta(0, t_k)}{\theta_i} \right] \frac{r_0^2}{2.4048^2 \alpha} \quad (24)$$

466 The characteristic time  $t_k$  defined in Eq. (24) is the time at which the temperature difference among the fluid at the cylinder  
 467 axis and the wall,  $\theta(0, t_k)$ , has been reduced to a certain ratio of the initial difference.  
 468 Please note that, from the definition of Eq. (19), the  $\tau_{Ad}$  ratio defined to assess the problem is proportional to the Fourier  
 469 number:

$$\tau_{Ad} = \frac{t_{res}}{t_k} = K_{Ad} \frac{\alpha t_{res}}{r_0^2} = K_{Ad} Fo \quad (25)$$

470 where  $K_{Ad}$  is a constant for the transient radial heat conduction through an injector duct that depends on the problem  
 471 eigenvalue and the considered ratio among the wall temperature and the fuel temperature at the duct axis. As a remark,  
 472 the appearance of  $Fo$  is aligned with the interpretation of  $\tau_{Ad}$  given earlier, since low values of  $Fo$  imply that the heat  
 473 transfer is still at its transient stage, whereas high values of  $Fo$  imply that steady temperatures are reached and the heat  
 474 transfer process has been completed.

475 *4.2.2. Estimation for engine-like and laboratory characteristic conditions*

476 Once the parameter  $\tau_{Ad}$  has been theoretically defined to qualitatively assess the relevance of heat transfer during the  
477 injection process, it is interesting to evaluate it for realistic operating conditions for which experimental data are available:

- 478 • Characteristic operating points of a typical passenger car diesel engine are considered. The main characteristics  
479 of this 4 cylinder and 1.9 l engine summarized in **Table 2**. Combinations of engine speeds ( $n_e$ ) from 1250 to  
480 4000 rpm and BMEPs from 3 to 21 bar (representative of the engine load) are taken into account, for a total  
481 sweep of 28 engine points. This engine was tested at these operating conditions in different previous works [55–  
482 57].
- 483 • The conditions reproduced in a laboratory environment to measure the rate of injection (ROI) of the Bosch CRI  
484 2.20 injector (which are part of the data used for the model validation described in the second part of the paper  
485 [30]) are evaluated as well. Experimental data of rate of injection are available from a previous work by the  
486 authors for a wide range of operating conditions [38]. These include injection pressures ( $p_i$ ) from 40 to 180 MPa,  
487 values of fuel temperature at the injector inlet ( $T_i$ ) from 253 to 373 K and energizing times (ET) from 0.25 ms  
488 to 2 ms. A total of 16 operating conditions were considered for each value of  $T_i$  tested.
- 489 • Similarly, conditions typically used to gather spray visualization data are also taken into account. This kind of  
490 measurements are usually performed in constant-pressure flow or constant-volume preburn vessels and include  
491 the determination of liquid-phase and vapor-phase penetration, lift-off length and ignition delay [58]. The same  
492 thermodynamic conditions stated for the ROI measurements are considered, with energizing times (ET) ranging  
493 from 0.5 to 2 ms in this case, since steady-state conditions are usually sought in the visualization studies.

Engine type	4-cylinder, 4-stroke
Displaced volume	1.9 l
Number of valves/cylinder	4
Stroke	90.4 mm
Bore	82 mm
Geometric compression ratio	17.5:1
Air management	Turbocharged
Maximum power	110 kW @ 4000 rpm
Maximum torque	315 Nm @ 2000 rpm
Injection	Common-rail DI

494 Table 2. Engine technical data.

495 As a reference for the fuel residence time ( $t_{res}$ ), the time needed for the injector to fully evacuate a fuel volume equivalent  
496 to the one of its internal lines has been considered. In the case of the Bosch CRI 2.20 injector, the dimensional  
497 characterization carried out to build the previous isothermal version of the model provided an approximate value of 6 cm<sup>3</sup>  
498 [18] for this volume. For each of the operating conditions tested, the mass injected per stroke ( $m_i$ ) is known, leading to a  
499 certain number of injections being necessary to evacuate the injector volume. If the injection frequency is known,  $t_{res}$  can

500 be easily estimated. In a four-stroke diesel engine, the injection frequency is half of the engine speed. In the case of the  
 501 ROI measurements used as a basis for the study, the injection frequency was set to 10 Hz, which is standard in laboratory  
 502 environments to avoid the influence of one injection on the next one. In the case of the spray visualization measurements,  
 503 lower injection frequencies are used so that the optical accesses are clear prior to each injection event. An injection  
 504 frequency of 0.25 Hz has been chosen as representative of this kind of measurement, since it has been used by the authors  
 505 [59] in the frame of the Engine Combustion Network group (ECN [60]) baseline measurements. For illustrating purposes,  
 506 **Table 3** shows a sample of the determination of  $t_{res}$  for 3 of the characteristic operating conditions that have been assessed  
 507 for each type of usage given to the injector.

Engine-like conditions						
Condition	$n_e$ [rpm]	BMEP [bar]	$m_i$ [mg/st]	No. injections [-]	$t_{res}$ [s]	
Low speed and load	1250	3.2	11.04	463	44.4	
Maximum torque	2000	20.7	59.69	86	5.2	
Maximum power	4000	15.4	48.22	106	3.2	
Laboratory measurements conditions					ROI	Spray visualization
Condition	$p_i$ [MPa]	ET [ms]	$m_i$ [mg/st]	No. injections [-]	$t_{res}$ [s]	$t_{res}$ [s]
Low pressure, short	40	0.5	5.25	972	97.2	3888
Medium pressure, long	120	1.0	44.33	116	11.6	464
High pressure, long	180	2.0	116.14	44	4.4	176

508 Table 3. Sample of  $t_{res}$  (time needed for the injector to evacuate a fuel volume equivalent to its own internal volume) for  
 509 different engine and laboratory characteristic conditions ( $T_i = 303$  K).

510 As far as the characteristic time of heat transfer due to conduction ( $t_k$ ) is concerned, it has been seen through the theoretical  
 511 analysis on the cylindrical duct that it depends on the fuel thermal diffusivity ( $\alpha$ ) and a characteristic diameter ( $r_0$ ).  $\alpha$  has  
 512 been evaluated from  $\rho_f$ ,  $c_p$  (see Section 3.1) and  $k_f$  (extracted from the literature for a standard diesel fuel [61]) for each  
 513 operating condition considered in the study. The duct feeding the injector nozzle and surrounding the needle has been  
 514 taken as a reference for the cylinder  $r_0$  due to its high volume (it accounts for most of the injector volume) and its influence  
 515 on the internal nozzle flow. The hydraulic diameter of the actual annular duct changes progressively (see **Figure 1**). The  
 516 section with an average hydraulic diameter (3.84 mm) has been considered representative of the problem for the  
 517 qualitative evaluation of  $t_k$ , leading to  $r_0 \approx 1.9$  mm. As shown in Eq. (24), the value of  $t_k$  depends on the reduction in the  
 518 initial difference among the wall temperature and the fluid temperature at the centre of the nozzle feeding line that is  
 519 considered as a reference.

520 **Table 4** shows the evaluation of  $t_k$  from Eq. (24) for several values of reduction of the temperature difference between  
 521 the fuel centreline and the wall ( $\theta$ ) non-dimensionalized with the initial temperature difference ( $\theta_i$ ). As stated earlier, it is  
 522 important to note that  $t_k$  has also been evaluated through a specific simulation of the transient heat transfer on the actual  
 523 annular geometry of the Bosch CRI 2.20 injector nozzle feeding line. In the simulation, both the inner and the outer walls

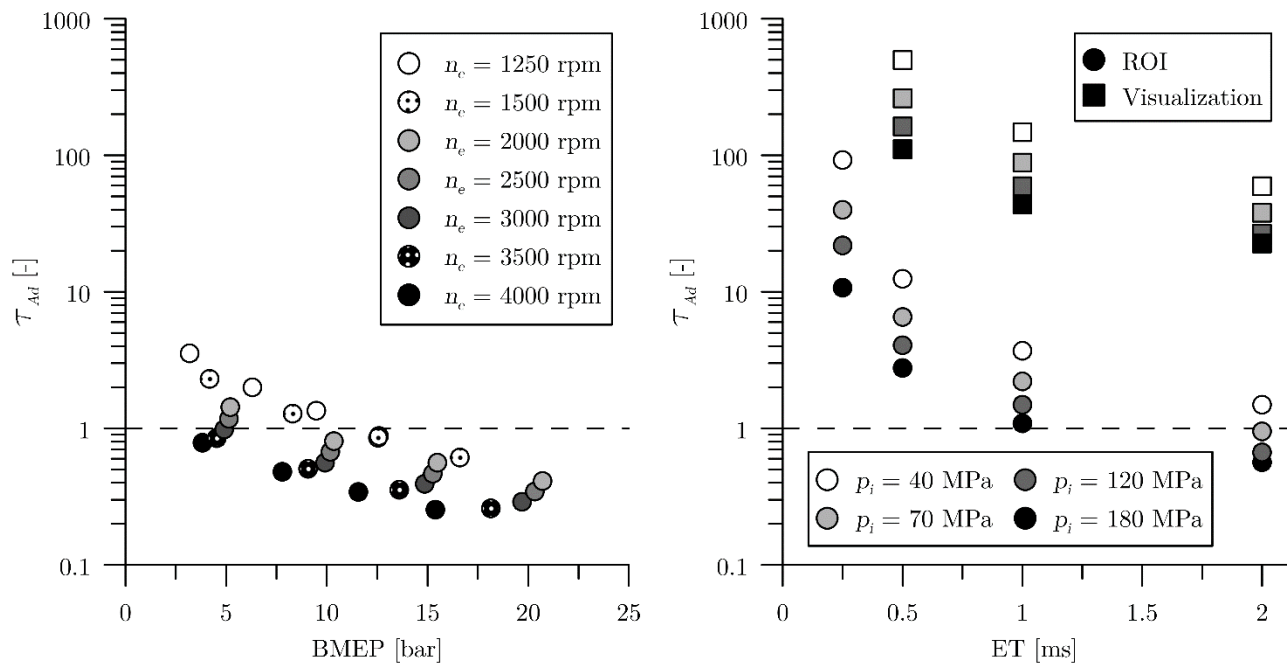
524 of the duct are set to a constant temperature  $T_w$  different from the initial fuel temperature  $T_i$ . Results in this case are also  
 525 shown in **Table 4**, with  $\theta$  evaluated at the location where the fuel temperature difference is maximum (analogous to the  
 526 cylindrical case, where the maximum temperature difference occurs at the centreline). The comparison among the studied  
 527 geometries shows that the characteristic times always differ by a factor lower than 1.5, implying that the geometry chosen  
 528 to compute  $\tau_{Ad}$  will not impact the order of magnitude of the estimations and the validity of the associated qualitative  
 529 analysis. The cylindrical duct case is then considered hereinafter. A ratio  $\theta/\theta_i = 0.3678$  (corresponding to the number  
 530  $e^{-1}$ ) has been selected as a reference for  $t_k$  since it leads to the logarithm in Eq. (24) being cancelled, which is a standard  
 531 in the definition of relaxation times. Please note that, in the view of the values shown in Table 4, this arbitrary choice of  
 532  $t_k = 7.34$  s is not expected to modify the order of magnitude of  $\tau_{Ad}$  and the conclusions stated in this section either.

$\theta/\theta_i$ (%) [-]	$t_k$ [s]	
	Cylindrical duct (Eq. 24)	Annular duct (simulated)
75	2.24	2.35
50	5.41	4.22
36.78	<b>7.34</b>	5.61
20	11.82	8.37
10	16.91	11.5
5	22.0	14.63

533 Table 4. Estimation of  $t_k$  for several values of the ratio among  $\theta$  and  $\theta_i$ , both for the cylindrical duct theoretical case and  
 534 the simulated annular duct case.

535 According to Eq. (19),  $\tau_{Ad}$  can now be evaluated from the estimations of  $t_{res}$  and  $t_k$ . This parameter is depicted in Figure  
 536 **5(a)** as a function of the engine-like operating conditions (engine speed and load), whereas it is shown for the conditions  
 537 of the ROI and visualization measurements (injection pressure and energizing time) corresponding to a reference value  
 538 of  $T_i = 303$  K in Figure **5(b)**.





539

(a) Engine-like conditions.

(b) Laboratory measurements conditions.

540 Figure 5. Estimation of  $\tau_{Ad}$  for engine-like conditions corresponding to different values of engine speed and load (a) and  
 541 for typical conditions of laboratory measurements including different values of injection pressure and ET (b).

542 Results of Figure 5(a) show that  $\tau_{Ad}$  is higher than 1 for the lowest engine speeds and lowest engine loads, being lower  
 543 than 1 for all engine speeds in the case of medium to high engine loads. For the low to medium engine loads,  $\tau_{Ad}$  also gets  
 544 lower than 1 from a certain intermediate value of engine speed. In any case,  $\tau_{Ad}$  always remains within the orders of  
 545 magnitude closer to 1 ( $0.1 < \tau_{Ad} < 10$ ). Therefore, the order of magnitude of the fuel residence time within the injector is  
 546 similar to the one for the characteristic time of heat transfer with the surroundings by conduction. As stated earlier this  
 547 implies that, in these conditions, heat transfer seems to be relevant to a certain extent. Thus, the temperature of the fuel  
 548 inside the injector has enough time to get closer to the injector wall temperature prior to each injection event, departing  
 549 from the initial fuel temperature right at the injector inlet. In any case, the heat transfer process among injections will still  
 550 be at its transient stage by the time of a new injection and the fuel temperature is not expected to have reached the wall  
 551 temperature completely. Prior to each injection, the fuel temperature will be more similar to the wall temperature for the  
 552 lowest engine speeds and loads ( $1 < \tau_{Ad} < 10$ ), whereas its change from the fuel initial temperature will be less accused  
 553 (but existent) the higher the engine speed and the engine load ( $0.1 < \tau_{Ad} < 1$ ). During a given injection, however, since the  
 554 wall temperature and the fuel temperature will already be closer to each other, the considerations previously given about  
 555 the adiabatic assumption with the  $Ad$  number are valid: if the  $Ad$  number (established by both the geometry of each injector  
 556 restriction and the induced operating conditions) is high (as it has been shown for the Bosch CRI 2.20 injector orifices in  
 557 steady-state conditions), the already low temperature difference among fluid and wall will prevent the fuel from further

558 changing its temperature due to heat exchange. Only its own internal evolution due to the strong pressure drops established  
559 across the orifices will be able to modify the fuel temperature. Hence, the assumption of adiabatic flow during an injection  
560 may still hold with the particularity that a certain temperature gap should be initially considered for  $T_i$  prior to each  
561 injection (again, this gap is more accused for the lowest engine speeds and loads). This finding is particularly useful to  
562 set up computational simulations or to adjust correlations of certain variables based on experimental measurements. On  
563 the contrary, if the  $Ad$  number is low (as it may happen during the transient operation of the injector where the pressure  
564 gradients in the orifice are still low), the temperature changes along the injector cannot be solely explained by the pressure  
565 drops across the injector internal orifices and will be partially due to heat exchange with the surroundings. Moreover, for  
566 low values of  $Ad$ , the flow regime across the injector ducts would probably be laminar, with the laminar boundary layer  
567 additionally slowing down the flow close to the injector walls and reinforcing the heat exchange relevance.

568 As far as the laboratory measurements conditions depicted in Figure 5(b) are concerned,  $\tau_{Ad}$  decreases with the injection  
569 pressure and the injector energizing time, as expected. Focusing on the ROI measurements conditions, similar conclusions  
570 to the ones found for the engine-like conditions can be extracted in the view of the results. Nevertheless, some operating  
571 conditions lead to a different order of magnitude for  $\tau_{Ad}$  ( $10 < \tau_{Ad} < 100$ ). In particular, the shortest injections fall in this  
572 regime. This means that, under these conditions, the heat transfer process is practically completed by the time of a new  
573 injection. In these cases, it is accurate to assume that the fuel temperature already matches the wall temperature prior to  
574 each injection. During the injection itself, the low temperature difference among the wall and the fluid could lead again  
575 to heat exchange being negligible. The magnitude of the temperature change across the internal restrictions of the injector  
576 would depend on the induced  $Ad$  values, as explained earlier. In any case, it is important to note that the results presented  
577 correspond to an injection frequency of 10 Hz. The conclusions could differ if a different injection frequency was selected.

578 In fact,  $\tau_{Ad}$  is an order of magnitude larger for the laboratory conditions sought in spray visualization measurements, with  
579 an injection frequency of 0.25 Hz. Several conditions fall in the regime corresponding to  $100 < \tau_{Ad} < 1000$ . In these  
580 conditions, it is accurate to assume that the initial fuel temperature at the injector inlet completely matches the wall  
581 temperature. This result will be of interest to experimentalists that insulate the injector holder for their measurements  
582 seeking to control the fuel injection temperature. Again, no relevant heat transfer would take place during the injection as  
583 long as the induced values of  $Ad$  were high, so that the fuel temperature evolution from the injector inlet to the nozzle  
584 outlet could be estimated with the adiabatic flow hypothesis as introduced in Section 3. These results are analysed with  
585 the implemented computational model in the second part of the paper [30].

586 Therefore, from the results of Figure 5(b) it follows that several options are available if the influence of heat transfer

587 wanted to be isolated when designing a laboratory experiment. On the one hand, the laboratory user may directly control  
588 the relative importance of heat transfer in the injection process through the injection frequency. On the other hand, this  
589 issue can also be manipulated by properly selecting the ET of the injections.

590 It is important to give some remarks about the limitations of this study. The proposed limiting case behaviour (with the  
591 implications of  $t_{Ad}$  being lower, equal or greater than 1) can only give an idea on the qualitative importance of the different  
592 phenomena involved in the process, being reliable only in terms of orders of magnitude. Some relevant phenomena cannot  
593 be captured by a single time  $t_k$  to account for conduction from injector walls to fuel. For instance, in the real application,  
594 important temperature gradients may be present along the injector walls given the higher temperatures at which the nozzle  
595 tip is submitted, as opposed to the rest of the injector body. These temperature gradients may differ depending on the  
596 duration of the engine run. However, this could only be accounted for through a model with yet more uncertainties that  
597 would hinder the analysis of results. In any case, this fact is not deemed to condition the order of magnitude of the results  
598 here presented and their qualitative interpretation.

## 599 5. CONCLUSIONS

600 The introduction of the hypothesis of adiabatic flow to account for local temperature variations in the computational  
601 model of a common-rail solenoid diesel injector has been dealt with in this work. The main features of the model have  
602 been described, focusing on the implementation of the hypothesis on a previous version of the model (which employed  
603 the isothermal flow assumption) and the qualitative assessment of its validity. To do so, two non-dimensional parameters  
604 have been analysed to estimate the importance of the heat transfer processes both during the injection and in the time  
605 lapse among injections. The main findings of the present work are summarized as follows:

- 606 • The adiabatic flow hypothesis implies that the fuel temperature change along an injector hydraulic restriction  
607 (such as an orifice) depends on the pressure drop and the velocity change (which in the end is related to the  
608 discharge coefficient) through the restriction. If the flow velocity remained constant along an adiabatic process,  
609 the conservation of fuel specific enthalpy would imply a heating upon expansion.
- 610 • During the injection, the proneness of the flow along the injector to exchange heat with the surroundings depends  
611 on a non-dimensional quantity ( $Ad$ ) that is a function of the orifice diameter-to-length ratio,  $Re$  and  $Nu$ .  
612 Consequently, for the injector of study it was found that heat transfer may be relevant when low values of  $Re$  are  
613 induced. This is the case of the transient stages (opening and closing), for which large pressure drops along the  
614 injector orifices are still not established.
- 615 • The heat exchange process existing in the time lapse among injections has been analysed by means of a non-

616 dimensional parameter ( $\tau_{Ad}$ ) proportional to  $Fo$  that compares the fuel residence times within the injector to a  
617 characteristic time of heat transfer. This characteristic time has been assessed with the simplified case of transient  
618 radial conduction in an infinitely long cylinder (although its assessment through a simulation conducted for a  
619 more realistic injector duct proved to lead to the same qualitative conclusions). The evaluation of  $\tau_{Ad}$  for typical  
620 engine operating conditions shows that the heat transfer process is generally still at its transient stage prior to  
621 each injection. Thus, heat transfer is relevant to a certain extent and, by the time of a new injection, the fuel  
622 temperature is not expected to have reached the injector wall temperature completely. In any case, the lower the  
623 engine speed and load, the closer these two temperatures will get to each other before each injection. The findings  
624 were similar when evaluating  $\tau_{Ad}$  for the usual operating conditions of the ROI measurements typically performed  
625 in a laboratory environment, with the exception of the short injections. In this case, as it also happens with the  
626 usual conditions of visualization experiments, the high residence times associated to the injections imply that the  
627 heat transfer process will be completed prior to each injection, resulting in the fuel temperature at the injector  
628 inlet being equal to the injector wall temperature.

629 • In the case of laboratory measurements, the injection frequency and the injection energizing time play a key role  
630 on the heat transfer processes. This fact may be used to the advantage of the researcher when designing a new  
631 experiment, since these conditions may be selected so that heat transfer only occurs either during the injection  
632 or in the time lapse among injections and its influence is isolated from the study. On the one hand, using high  
633 injection frequencies (or large energizing times) reduces the fuel residence time within the injector, so that the  
634 heat transfer in the lapse among injections becomes negligible. In this case, any heat transfer would take place  
635 during the injector opening and closing (where low values of  $Ad$  are present), whose relative importance in the  
636 injection event is lower the higher the energizing time. On the other hand, using low injection frequencies (or  
637 short energizing times) leads to the heat transfer process among injections being completed so that by the time  
638 of a new injection the fuel temperature already matches the wall temperature. In this case, no relevant heat  
639 transfer would take place during the injection as long as the induced values of  $Ad$  were high.

640 • The previous conclusion implies that the fuel temperature changes along the injector in steady-state conditions  
641 could be reasonably predicted through the use of the adiabatic flow hypothesis. Even if heat transfer was relevant  
642 during the time lapse among injections, the assumption of adiabatic flow could hold during the injection. This  
643 means that a computational model (or an experimental correlation depending on fuel properties) can be reliable  
644 if a certain temperature gap is considered for the fuel temperature and its associated properties at the injector

645 inlet prior to each injection.

646

## 647 **ACKNOWLEDGEMENTS**

648 This work was partly sponsored by FEDER and the Spanish “Ministerio de Economía y Competitividad” in the frame of  
649 the project “Desarrollo de modelos de combustión y emisiones HPC para el análisis de plantas propulsivas de transporte  
650 sostenible (CHEST)”, reference TRA2017-89139-C2-1-R-AR. The support of General Motors Global Research and  
651 Development (US) concerning the experimental measurements in the engine is gratefully acknowledged by the authors.  
652 The authors would also like to thank José Enrique del Rey, Léo Thiercelin and Mariano Sánchez for their technical help.

653

## 654 **REFERENCES**

- 655 [1] Heywood JB. Internal Combustion Engine Fundamentals. vol. 21. 1988.
- 656 [2] Payri R, Salvador FJ, Gimeno J, De la Morena J. Influence of injector technology on injection and combustion  
657 development, Part 1: Hydraulic characterization. *Appl Energy* 2011;88:1068–74.  
658 doi:10.1016/j.apenergy.2010.10.012.
- 659 [3] Payri R, Salvador FJ, Gimeno J, De la Morena J. Influence of injector technology on injection and combustion  
660 development, Part 2: Combustion analysis. *Appl Energy* 2011;88:1130–9. doi:10.1016/j.apenergy.2010.10.012.
- 661 [4] Gavaises M. Flow in valve covered orifice nozzles with cylindrical and tapered holes and link to cavitation  
662 erosion and engine exhaust emissions. *Int J Engine Res* 2008;9:435–47.
- 663 [5] Som S, Ramírez AI, Longman DE, Aggarwal SK. Effect of nozzle orifice geometry on spray, combustion, and  
664 emission characteristics under diesel engine conditions. *Fuel* 2011;90:1267–76. doi:10.1016/j.fuel.2010.10.048.
- 665 [6] Salvador FJ, Carreres M, Jaramillo D, Martínez-López J. Analysis of the combined effect of hydrogrinding  
666 process and inclination angle on hydraulic performance of diesel injection nozzles. *Energy Convers Manag*  
667 2015;105:1352–65. doi:10.1016/j.enconman.2015.08.035.
- 668 [7] Nguyen D, Duke D, Kastengren A, Matusik K, Swantek A, Powell CF, et al. Spray flow structure from twin-  
669 hole diesel injector nozzles. *Exp Therm Fluid Sci* 2017;86:235–47. doi:10.1016/j.expthermflusci.2017.04.020.
- 670 [8] Salvador FJ, de la Morena J, Carreres M, Jaramillo D. Numerical analysis of flow characteristics in diesel  
671 injector nozzles with convergent-divergent orifices. *Proc Inst Mech Eng Part D J Automob Eng*  
672 2017;231:1935–44. doi:10.1177/0954407017692220.
- 673 [9] Lee CS, Lee KH, Reitz RD, Park SW. Effect of split injection on the macroscopic development and atomization

- 674 characteristics of a diesel spray injected through a common-rail system. *At Sprays* 2006;16:543–62.  
675 doi:10.1615/AtomizSpr.v16.i5.50.
- 676 [10] Wang X, Huang Z, Zhang W, Abiola O, Nishida K. Effects of ultra-high injection pressure and micro-hole  
677 nozzle on flame structure and soot formation of impinging diesel spray. *Appl Energy* 2011;88:1620–8.  
678 doi:10.1016/j.apenergy.2010.11.035.
- 679 [11] Gumus M, Sayin C, Canakci M. The impact of fuel injection pressure on the exhaust emissions of a direct  
680 injection diesel engine fueled with biodiesel-diesel fuel blends. *Fuel* 2012;95:486–94.  
681 doi:10.1016/j.fuel.2011.11.020.
- 682 [12] Bianchi GM, Falfari S, Pelloni P, Kong S-C, Reitz RD. Numerical Analysis of High-Pressure Fast-Response  
683 Common Rail Injector Dynamics. *SAE Tech Pap* 2002-01-0213 2002. doi:10.4271/2002-01-0213.
- 684 [13] Marcer R, Audiffren C, Viel A, Bouvier B, Walbott A, Argueyrolles B. Coupling 1D System AMESim and 3D  
685 CFD EOLE models for Diesel Injection Simulation Renault. *ILASS - Eur. 2010, 23rd Annu. Conf. Liq. At.*  
686 *Spray Syst.*, 2010, p. 1–10.
- 687 [14] Arpaia A, Catania AE, Ferrari A, Spessa E. Development and Application of an Advanced Numerical Model for  
688 CR Piezo Indirect Acting Injection Systems. *SAE Tech Pap* 2010-01-1503 2010. doi:10.4271/2010-01-1503.
- 689 [15] Plamondon E, Seers P. Development of a simplified dynamic model for a piezoelectric injector using multiple  
690 injection strategies with biodiesel/diesel-fuel blends. *Appl Energy* 2014;131:411–24.  
691 doi:10.1016/j.apenergy.2014.06.039.
- 692 [16] Salvador FJ, Gimeno J, De la Morena J, Carreres M. Using one-dimensional modeling to analyze the influence  
693 of the use of biodiesels on the dynamic behavior of solenoid-operated injectors in common rail systems: Results  
694 of the simulations and discussion. *Energy Convers Manag* 2012;54:122–32.  
695 doi:10.1016/j.enconman.2011.10.007.
- 696 [17] Salvador FJ, Plazas AH, Gimeno J, Carreres M. Complete modelling of a piezo actuator last-generation injector  
697 for diesel injection systems. *Int J Engine Res* 2014;15:3–19. doi:10.1177/1468087412455373.
- 698 [18] Payri R, Salvador FJ, Carreres M, De la Morena J. Fuel temperature influence on the performance of a last  
699 generation common-rail diesel ballistic injector. Part II: 1D model development, validation and analysis. *Energy*  
700 *Convers Manag* 2016;114:376–91. doi:10.1016/j.enconman.2016.02.043.
- 701 [19] Wang X, Huang Z, Kuti OA, Zhang W, Nishida K. Experimental and analytical study on biodiesel and diesel  
702 spray characteristics under ultra-high injection pressure. *Int J Heat Fluid Flow* 2010;31:659–66.

- 703 doi:10.1016/j.ijheatfluidflow.2010.03.006.
- 704 [20] Theodorakakos A, Strotos G, Mitroglou N, Atkin C, Gavaises M. Friction-induced heating in nozzle hole  
705 micro-channels under extreme fuel pressurisation. *Fuel* 2014;123:143–50. doi:10.1016/j.fuel.2014.01.050.
- 706 [21] Strotos G, Koukouvinis P, Theodorakakos A, Gavaises M, Bergeles G. Transient heating effects in high  
707 pressure Diesel injector nozzles. *Int J Heat Fluid Flow* 2015;51:257–67.  
708 doi:10.1016/j.ijheatfluidflow.2014.10.010.
- 709 [22] Salvador FJ, Carreres M, De la Morena J, Martínez-Miracle E. Computational assessment of temperature  
710 variations through calibrated orifices subjected to high pressure drops: Application to diesel injection nozzles.  
711 *Energy Convers Manag* 2018;171:438–51. doi:10.1016/j.enconman.2018.05.102.
- 712 [23] Desantes JM, Salvador FJ, Carreres M, Jaramillo D. Experimental Characterization of the Thermodynamic  
713 Properties of Diesel Fuels Over a Wide Range of Pressures and Temperatures. *SAE Int J Fuels Lubr*  
714 2015;8:2015-01–0951. doi:10.4271/2015-01-0951.
- 715 [24] Dernette J, Hespel C, Foucher F, Houillé S, Mounaïm-Rousselle C. Influence of physical fuel properties on the  
716 injection rate in a Diesel injector. *Fuel* 2012;96:153–60. doi:10.1016/j.fuel.2011.11.073.
- 717 [25] Park Y, Hwang J, Bae C, Kim K, Lee J, Pyo S. Effects of diesel fuel temperature on fuel flow and spray  
718 characteristics. *Fuel* 2015;162:1–7. doi:10.1016/j.fuel.2015.09.008.
- 719 [26] Seykens X, Somers LMT, Baert RSG. Modelling of common rail fuel injection system and influence of fluid  
720 properties on process. *Proc. VAFSEP, Dublin, Ireland; July 6-9, 2004, p. 6–9.*
- 721 [27] Catania AE, Ferrari A, Spessa E. Temperature variations in the simulation of high-pressure injection-system  
722 transient flows under cavitation. *Int J Heat Mass Transf* 2008;51:2090–107.  
723 doi:10.1016/j.ijheatmasstransfer.2007.11.032.
- 724 [28] Yu H, Goldsworthy L, Brandner PA, Li J, Garaniya V. Modelling thermal effects in cavitating high-pressure  
725 diesel sprays using an improved compressible multiphase approach. *Fuel* 2018;222:125–45.  
726 doi:10.1016/j.fuel.2018.02.104.
- 727 [29] Salvador FJ, Gimeno J, Carreres M, Cialesi-Esposito M. Experimental assessment of the fuel heating and the  
728 validity of the assumption of adiabatic flow through the internal orifices of a diesel injector. *Fuel*  
729 2017;188:442–51. doi:10.1016/j.fuel.2016.10.061.
- 730 [30] Payri R, Salvador FJ, Carreres M, Belmar-Gil M. Thermal effects on the diesel injector performance through  
731 adiabatic 1D modelling. Part II: Model validation, results of the simulations and discussion. *Fuel* 2019;In

- 732 review.
- 733 [31] LMS. Imagine.Lab AMESim v.10. User's manual 2010.
- 734 [32] Salvador FJ, Gimeno J, De la Morena J, Carreres M. Comparison of Different Techniques for Characterizing  
735 the Diesel Injector Internal Dimensions. *Exp Tech* 2018;42:467–72. doi:10.1007/s40799-018-0246-1.
- 736 [33] Desantes JM, Lopez JJ, Carreres M, López-Pintor D. Characterization and prediction of the discharge  
737 coefficient of non-cavitating diesel injection nozzles. *Fuel* 2016;184:371–81. doi:10.1016/j.fuel.2016.07.026.
- 738 [34] Leonhard R, Warga J, Pauer T, Rückle M, Schnell M. Solenoid common-rail injector for 1800 bar. *MTZ*  
739 *Worldw* 2010;71:10–5. doi:10.1007/BF03227003.
- 740 [35] Payri R, Garcia-Oliver JM, Salvador FJ, Gimeno J. Using spray momentum flux measurements to understand  
741 the influence of diesel nozzle geometry on spray characteristics. *Fuel* 2005;84:551–61.  
742 doi:10.1016/j.fuel.2004.10.009.
- 743 [36] Siebers DL. Scaling liquid-phase fuel penetration in diesel sprays based on mixing-limited vaporization. *SAE*  
744 *Tech Pap* 1999-01-0528 1999. doi:10.4271/1999-01-0528.
- 745 [37] Desantes JM, Salvador FJ, Carreres M, Martínez-López J. Large-eddy simulation analysis of the influence of  
746 the needle lift on the cavitation in diesel injector nozzles. *Proc Inst Mech Eng Part D J Automob Eng*  
747 2014;229:407–23. doi:10.1177/0954407014542627.
- 748 [38] Salvador FJ, Gimeno J, Carreres M, Crialesi-Esposito M. Fuel temperature influence on the performance of a  
749 last generation common-rail diesel ballistic injector. Part I: Experimental mass flow rate measurements and  
750 discussion. *Energy Convers Manag* 2016;114:364–75. doi:10.1016/j.enconman.2016.02.042.
- 751 [39] Chorążewski M, Dergal F, Sawaya T, Mokbel I, Grolier JE, Jose J. Thermophysical properties of Normafluid  
752 (ISO 4113) over wide pressure and temperature ranges. *Fuel* 2013;105:440–50. doi:10.1016/j.fuel.2012.05.059.
- 753 [40] Huang D, Simon SL, McKenna GB. Chain length dependence of the thermodynamic properties of linear and  
754 cyclic alkanes and polymers. *J Chem Phys* 2005;122:84907. doi:10.1063/1.1852453.
- 755 [41] Bell IH, Wronski J, Quoilin S, Lemort V. Pure and pseudo-pure fluid thermophysical property evaluation and  
756 the open-source thermophysical property library coolprop. *Ind Eng Chem Res* 2014;53:2498–508.  
757 doi:10.1021/ie4033999.
- 758 [42] Růžička Jr V, Domalski ES. Estimation of the heat capacities of organic liquids as a function of temperature  
759 using group additivity. I. Hydrocarbon compounds. *J Phys Chem Ref Data* 1993;22:597–618.  
760 doi:10.1063/1.555923.



- 761 [43] Zábbranský M, Kolská Z, Růžička V, Domalski ES. Heat capacity of liquids: Critical review and recommended  
762 values. Supplement II. *J Phys Chem Ref Data* 2010;39:3–404. doi:10.1063/1.3182831.
- 763 [44] Kouzel B. How pressure affects liquid viscosity. *Hydrocarb Process Pet Refin* 1965;44 (3):120.
- 764 [45] Winklhofer E, Wiesler B, Ahmadi-Befrui B, Cresnoverh G. The influence of injection rate shaping on Diesel  
765 fuel sprays - an experimental study. *ImechE* 1992;206:173–83.
- 766 [46] Nishimura T, Satoh K, Takahashi S, Yokota K. Effects of Fuel Injection Rate on Combustion and Emission in a  
767 DI Diesel Engine. *SAE Tech. Pap.* 981929, 1998. doi:10.4271/981929.
- 768 [47] Benajes J, Molina S, De Rudder K, Rente T. Influence of Injection Rate Shaping on Combustion and Emissions  
769 for a Medium Duty Diesel Engine. *J Mech Sci Technol* 2006;20:1436–48.
- 770 [48] He Z, Xuan T, Xue Y, Wang Q, Zhang L. A numerical study of the effects of injection rate shape on  
771 combustion and emission of diesel engines. *Therm Sci* 2014;18:67–78. doi:10.2298/TSCI130810013H.
- 772 [49] Payri F, Payri R, Bardi M, Carreres M. Engine combustion network: Influence of the gas properties on the spray  
773 penetration and spreading angle. *Exp Therm Fluid Sci* 2014;53:236–43.  
774 doi:10.1016/j.expthermflusci.2013.12.014.
- 775 [50] Sieder EN, Tate GE. Heat Transfer and Pressure Drop of Liquids in Tubes. *Ind Eng Chem* 1936;28:1429–35.  
776 doi:10.1021/ie50324a027.
- 777 [51] Nusselt W. Der Wärmeaustausch zwischen Wand und Wasser im Rohr. *Forsch Auf Dem Gebiete Des*  
778 *Ingenieurwesens* 1931;2:309–13. doi:10.1007/BF02583210.
- 779 [52] Salvador FJ, Carreres M, Crialesi-Esposito M, Plazas AH. Determination of critical operating and geometrical  
780 parameters in diesel injectors through one dimensional modelling, design of experiments and an analysis of  
781 variance. *Proc Inst Mech Eng Part D J Automob Eng* 2018;232:1762–81. doi:10.1177/0954407017735262.
- 782 [53] Matsumoto S, Yamada K, Date K. Concepts and Evolution of Injector for Common Rail System. *SAE Tech Pap*  
783 2012-01-1753 2012. doi:10.4271/2012-01-1753.
- 784 [54] Schöppe D, Zülch S, Hardy M, Geurts D, Jorach RW, Baker N. Delphi Common Rail system with direct acting  
785 injector. *MTZ Worldw* 2008;69:32–8. doi:10.1007/BF03226918.
- 786 [55] Benajes J, Olmeda P, Martín J, Blanco-Cavero D, Warray A. Evaluation of swirl effect on the Global Energy  
787 Balance of a HSDI Diesel engine. *Energy* 2017;122:168–81. doi:10.1016/j.energy.2017.01.082.
- 788 [56] Broatch A, Olmeda P, García A, Salvador-Iborra J, Warray A. Impact of swirl on in-cylinder heat transfer in a  
789 light-duty diesel engine. *Energy* 2017;119:1010–23. doi:10.1016/j.energy.2016.11.040.

- 790 [57] Broatch A, Martín J, García A, Blanco-Cavero D, Warray A, Domenech V. Application of a zero-dimensional  
791 model to assess the effect of swirl on indicated efficiency. *Int J Engine Res* 2018;In press.  
792 doi:10.1177/1468087418779726.
- 793 [58] Bardi M, Payri R, Malbec L-M, Bruneaux G, Pickett LM, Manin J, et al. Engine Combustion Network:  
794 Comparison of Spray Development, Vaporization, and Combustion in Different Combustion Vessels. *At Sprays*  
795 2012;22:807–42. doi:10.1615/AtomizSpr.2013005837.
- 796 [59] Gimeno J, Martí-Aldaraví P, Carreres M, Peraza JE. Effect of the nozzle holder on injected fuel temperature for  
797 experimental test rigs and its influence on diesel sprays. *Int J Engine Res* 2018;19:374–89.  
798 doi:10.1177/1468087417751531.
- 799 [60] ECN. Engine Combustion Network. <https://EcnSandiaGov/Diesel-Spray-Combustion/> 2010.  
800 [www.sandia.gov/ecn/](http://www.sandia.gov/ecn/).
- 801 [61] Kolev NI. Thermodynamic and transport properties of diesel fuel. *Multiph. Flow Dyn. 3 Turbul. gas Absorpt.*  
802 release, diesel fuel Prop. 3rd editio, Springer Verlag; 2007, p. 293–327.
- 803